OLEDs

DOI: 10.1002/anie.201303031

Solution Processed Organic Double Light-Emitting Layer Diode Based on Cross-Linkable Small Molecular Systems**

*Georgios Liaptsis, Dirk Hertel, and Klaus Meerholz**

Dedicated to the Bayer company on the occasion of its 150th anniversary

State-of-the-art organic light-emitting diodes (OLEDs) consist of a multi-layer device structure to ensure higher power conversion efficiencies and extended lifetimes compared to their single-layer counterparts.[1] The use of phosphorescent emitters based on transition metal complexes such as Pt^{II} [2] or Ir^{III} compounds[3] has led to quantum yields close to unity through their effective inter-system crossing rate from excited singlet states to highly emissive triplet states.[4] Losses in radiative decay caused by triplet–triplet annihilation and aggregation quenching of excited states can be suppressed by the introduction of a host–guest system as the emitting layer (EML).[5] The energy-level arrangement of the host and the guest must energetically fit in regards to charge-carrier injection and Förster[6] and/or Dexter[7] type energy transfer from excited host molecules to the emitting guest molecules. Thus, efficient triplet harvesting on the emitting molecules is accomplished.[8] An advanced concept to enhance the efficiency of phosphorescent OLEDs (PHOLEDs) is the implementation of a charge-carrier accumulating interface inside the EML. This idea is realized by so-called "double-emission layers" (DEL) which utilize two different host materials with the same guest emitter. They can reduce losses of triplet excitons into regions which are not doped by the phosphorescent material.[9]

To allow for cost-effective OLED production for solid-state lighting or display applications, solvent-based fabrication techniques, such as roll-to-roll or ink-jet printing, are favoured over more expensive vacuum-based deposition techniques.[10] When creating a multi-layer OLED from solution, it is important to prevent interface mixing and erosion during deposition of the subsequent layers. Besides orthogonal solvent processing[11] a well-established approach to prepare solvent-based multi-layer devices is the chemical functionalization of the organic semiconductors with reactive moieties for thermally polymerization[12] and/or cross-linking.[13] We have reported on cross-linkable oxetane-functionalized semiconductors, that can be cross-linked by cationic ring opening polymerization (CROP), which is induced by a photo acid generator (PAG), yielding an insoluble film after deposition and curing without degradation of the optoelectronic properties.[14] Herein, we present the first DEL–OLEDs fabricated entirely from solution using both, novel oxetane-functionalized host and phosphorescent guest materials. We report on the materials' synthesis, their optoelectronic characterization, and finally their use in OLED devices.

Regarding phosphorescent emitters, we focused on easy-to-synthesize, highly soluble, and cross-linkable tris-cyclometallated homo- and heteroleptic (*fac*)-Ir^{III} complexes derived from the established emitter *fac*-[Ir(mppy)$_3$], which is commonly used in OLEDs.[2a] We propose to replace the methyl group on the *p*-methylphenyl pyridine ligand by a diarylamine, yielding a pyridine-substituted triarylamine (TPA-Py) ligand. By doing so, the hole-trapping properties are improved. At the same time, the attachment of the cross-linkable oxetane unit by a C_6-spacer dramatically increases the solubility of the resulting complexes, reducing the tendency to self-aggregate and, thus, self-quench.

Synthesis, electrochemical, and spectroscopic characterization of the new emitters (X-IrG*n*, see Figure 1) are described in the Supporting Information. In short, all the complexes feature reversible oxidation (Figure S1), and the HOMO energy decreases with increasing number *n* of X-TPA-Py ligands from −5.25 eV for the reference compound *fac*-[Ir(mppy)$_3$] ($n=0$) to −5.14 eV for X-IrG3 ($n=3$), respectively (Table 1). This trend is caused by the increasing amount of donor-substituted ligands connected to the metal center. Compared to *fac*-[Ir(mppy)$_3$] the donor effect of the diphenylamine group increases the absorption coefficient of the metal-to-ligand charge transfer (MLCT) state and shifts the photoluminescence bathocromically.

The suitability of the new oxetane-functionalized complexes as emitters in OLEDs was first tested in solution-processed multi-layer PHOLEDs (see Figure 1 for structural formula and Figure 2 for device setup).[15] These devices are referred to as P1–P3 (containing X-IrG1–G3, respectively). For comparison, devices using the same layer sequence, but *fac*-[Ir(mppy)$_3$] as the emitter were fabricated (Figure 3 left; inverted triangles; device P0). As shown in Figure 3 left, device P1 performed best, reaching a luminous efficiency at a luminance of 1000 Cd m^{-2} (LE_{1000}) of 45.9 Cd A^{-1}, followed by P2 ($LE_{1000}=35.2$ Cd A^{-1}), and finally P3 ($LE_{1000}=22.9$ Cd A^{-1}). The reference device P0 reached slightly better performance under these conditions ($LE_{1000}=25.3$ Cd A^{-1}, however, at lower light output all novel com-

[*] Dr. G. Liaptsis, Dr. D. Hertel, Prof. Dr. K. Meerholz
Chemistry Department, University of Cologne
Luxemburger Strasse 116, 50939 Cologne (Germany)
E-mail: klaus.meerholz@uni-koeln.de
Homepage: http://www.meerholz.uni-koeln.de

[**] We acknowledge funding by the State of Northrhine-Westfalia and the Europäischer Fonds für Regionale Entwicklung (EFRE) through the PROTECT project, which is part of the Centre of Organic Production Technologies COPT.NRW.

Supporting information for this article is available on the WWW under http://dx.doi.org/10.1002/anie.201303031.

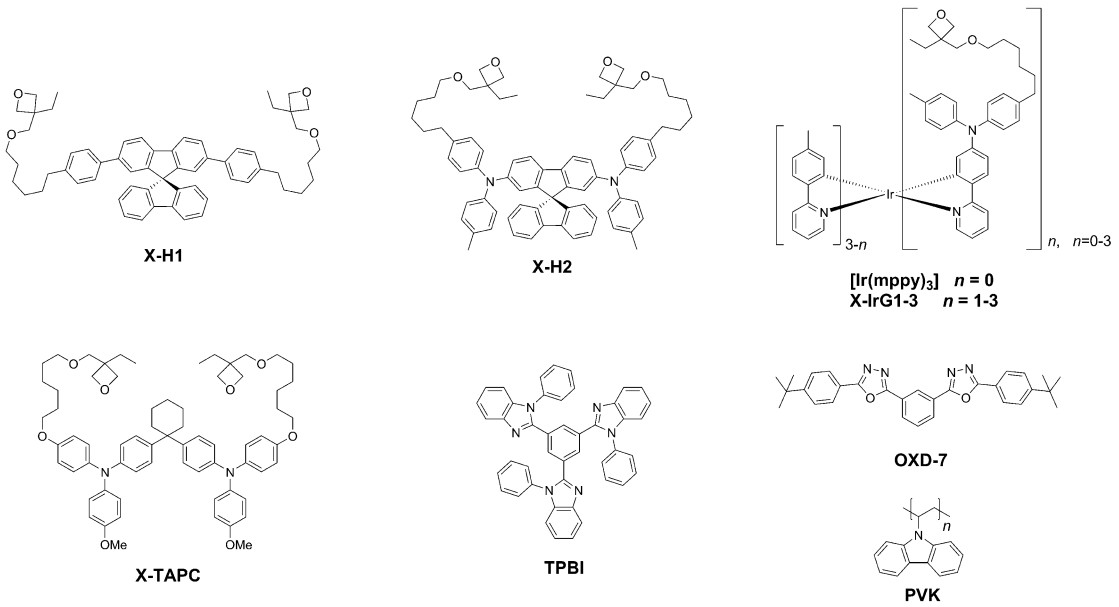

Figure 1. Structural formula of compounds used in this study. The top row: the novel cross-linkable host materials X-H1 and X-H2 as well as the phosphorescent green emitting materials *fac*-[Ir(mppy)$_3$] and X-IrG1–3. Bottom row: the additional compounds used in the devices P0–3, S1–2, and D, these are the cross-linkable hole conductor X-TAPC, the electron conductors 1,3-bis(5-(4-*tert*-butylphenyl)-1,3,4-oxadiazol-2-yl)benzene (OXD-7) and 1,3,5-tris(1-phenyl-1H-benzo[d]imidazol-2-yl)benzene (TPBI), as well as the host material poly(N-vinylcarbazole) (PVK).

Table 1: Summary of physical properties.[a]

Compound	E_{Ox} [V]	E_{HOMO} [eV]	λ_{edge} [nm]	E_{LUMO} [eV]	S_1 [eV]	T_1 [eV]	ΔE_{ST} [eV]
X-H1	0.93	−5.94	372	−2.61	3.06	2.27	0.79
X-H2	0.08	−5.17	435	−2.32	2.87	2.26	0.61
[Ir(mppy)$_3$]	0.17	−5.25	500	−2.61	–	2.45[15b]	–
X-IrG1	0.11	−5.20	500	−2.72	–	2.34	–
X-IrG2	0.05	−5.15	500	−2.77	–	2.34	–
X-IrG3	0.04	−5.14	500	−2.78	–	2.34	–
PVK	–	−5.90[27]	–	−2.20[27]	–	2.75[28]	–
OXD-7	–	−6.30[27]	–	−2.40[27]	–	2.70[27]	–
H1	0.93[20]	−5.94	–	−2.23	–	–	–
H2	0.19[29]	−5.27	396[29]	−2.14	–	–	–

[a] E_{Ox} is the oxidation potential determined by cyclic voltammetry referenced to the ferrocene/ferrocenium redox couple. E_{HOMO} is the HOMO energy calculated according to Equation (1). λ_{edge} is the bathochromic edge of absorption determined in THF solution and extracted on a logarithmic scale of the absorption data. E_{LUMO} is the LUMO energy. S_1 and T_1 are the first excited singlet and triplet states, respectively, wherein ΔE_{ST} is the difference between these values. The data of the parent host materials without cross-linkable side chains is mentioned for comparison. The HOMO energies were calculated as mentioned in the Supporting Information using the first oxidation potential versus the Ferrocene/Ferrocenium redox couple published in literature (Note that we used 0.48 V as potential for Fc/Fc^+ vs. Ag/AgCl electrode). The LUMO of H1 was calculated by the addition of the difference between the first oxidation and first reduction potential to the HOMO level. The LUMO of H2 was calculated by adding the band-gap energy to the HOMO level.

plexes clearly outperform the reference *fac*-[Ir(mppy)$_3$], which is also reflected in the turn-on voltage, decreasing in the sequence P1 < P2 < P3 ≪ P0. This improvement relative to the parent compound is clearly attributed 1) to an improved dispersion of the complexes within the matrix through higher solubility[16] and 2) to the improved hole transport and hole trapping on the complexes.[15b] Compared to *fac*-[Ir(mppy)$_3$] which has no X-TPA-Py ligand, X-IrG1 traps holes more efficiently and the attraction of electrons followed by the formation of excitons is improved.[17] On the other hand, the decreasing device performance with increasing amount of triphenylamine (TPA) subunits of X-IrG1–3 is explained by the competition between their hole trapping ability and their hole transport ability. An increase of TPA subunits enhances the hole mobility in the emitting layer, which has a negative impact on the device performance within this device series.[18] This result is confined by hole-only devices (Figure S5). More detailed device performance parameters are listed in the Supporting Information (Table S2).

In view of the excellent electroluminescent properties of the new emitters compared to a standard emitter such as *fac*-[Ir(mppy)$_3$], we searched for novel cross-linkable, bipolar host materials to enable the fabrication of multi-emitting-layer devices from solution. Compounds containing spirobifluorene as central building block appear to be promising candidates,[19] offering bipolar transport properties[20] in addition to small singlet–triplet splitting energies (ΔE_{ST}).[19c,21,22] A high-lying triplet state of the host is important to prevent the exothermic energy back transfer from the emissive triplet state of the emitting transition-metal complex to the non-emissive triplet state of the hydrocarbon host material during OLED operation.

Synthesis, electrochemical, and spectroscopic characterization of the new host materials X-H1 and X-H2 (see Figure 1) are described in Supporting Information. In short,

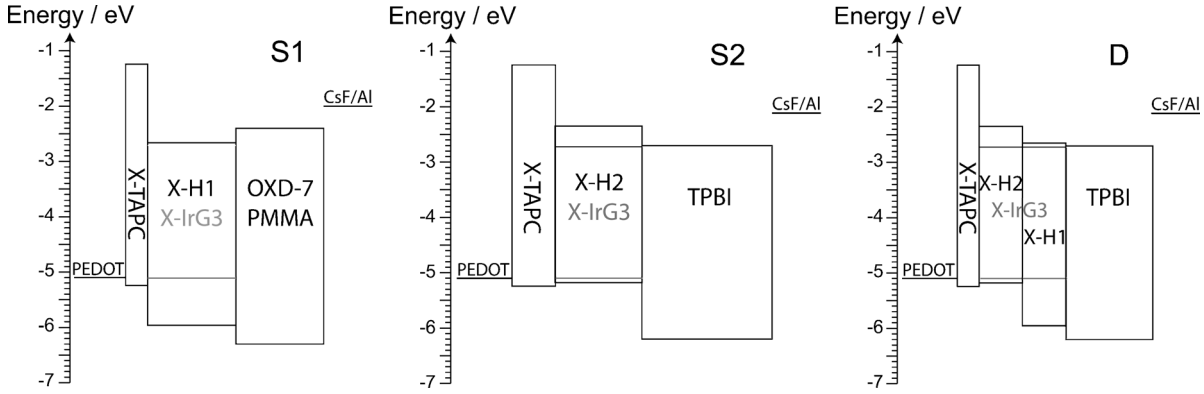

Figure 2. Energy level arrangement of the optimized devices S1 (left), S2 (middle), and D (right). The device S1 consists of X-TAPC (20 nm)//X-H1- X-IrG3 (8%) (40 nm)//OXD-7: PMMA (75:25) (40 nm)//CsF (2 nm)//Al (100 nm). The device S2 consists of X-TAPC (20 nm)//X-H2- X-IrG3 (8%) (40 nm)//TPBI (60 nm)//CsF (2 nm)//Al (100 nm). The device D consists of X-TAPC (10 nm)//X-H2- X-IrG3 (8%) (20 nm)//X-H1- X-IrG3 (8%) (20 nm)//TPBI (40 nm)//CsF (2 nm)//Al (100 nm).

the energy levels allow efficient charge injection and subsequent trapping in the Ir^{III} emitter. The materials form homogeneous films with a high photoluminescence quantum yield (PLQY) upon doping with the Ir^{III} complexes (Table S1).

Multi-layer OLEDs with state-of-the-art device stacks were fabricated. These devices were optimized towards high luminous efficiency by varying the emitter (X-IrG1–3) and the host (X-H1 or X-H2), the doping concentration of the emitter in the host (between 2.5 and 15.0 mole%), the cross-linking method (Figure S4) as well as the choice of electron-transport/hole-blocking material (TPBI or OXD-7 in PMMA; see Figure 1). As the hole-transport/electron-blocking layer we used X-TAPC, since its HOMO energy fits perfectly between the work function of PEDOT:PSS and the HOMO level of X-IrG3 (the performance of devices without X-TAPC was strongly reduced). Finally, the layer thicknesses d of all individual layers were optimized ($0 < d < 100$ nm). X-IrG3 generally performed slightly better than X-IrG1 and X-IrG2 because it has the lowest quenching rate of all three emitters after the cross-linking. Therefore, we focus on devices using X-IrG3 as the emitter. The optimum initial doping concentration of X-IrG3 in the emission layer was found to be 8 mole%. The structure of the optimized single-emission-layer OLEDs (SEL-OLED) based on the matrix materials X-H1 or X-H2, respectively (referred to as devices S1 and S2), and DEL–OLEDs (referred to as device D) are described in detail in Figure 2.

The OLED performance of the three devices is shown in Figure 3 right, more details are listed in Table S2. All devices turn on at rather low voltage (2.75–3.00 V). At low light output (under 10 $Cd\,m^{-2}$) device D shows the best performance, followed by devices S2 and S1, respectively. With increasing light output, the devices reach their maximum luminous efficiencies of $LE_{max} = 34$ (29) $Cd\,A^{-1}$ for the devices S2 and D (S1, respectively), however, the voltage to achieve this increases in the sequence $D < S2 < S1$. At the reference brightness of 1000 $Cd\,m^{-2}$ the three devices performed similarly, reaching $LE = (27.5 \pm 1)$ $Cd\,A^{-1}$. Finally, at higher brightness LE drops down dramatically, which is commonly observed in many triplet-based OLEDs and attributed to triplet–triplet annihilation[23] or triplet–polaron quenching.[24] The best performing device is D (12 $Cd\,A^{-1}$ at 8500 $Cd\,m^{-2}$), followed by S2 and S1, respectively, resulting from enhanced recombination of charge carriers at the interface between the two emission layers[9] and, as a result, a widening of the emission zone (EMZ) profile (see Table S2). It is important to note, that all cross-linked devices outperform the reference device P3, despite the fact that some of the emitter had degraded (ca. 40%; Figure S4). Thus,

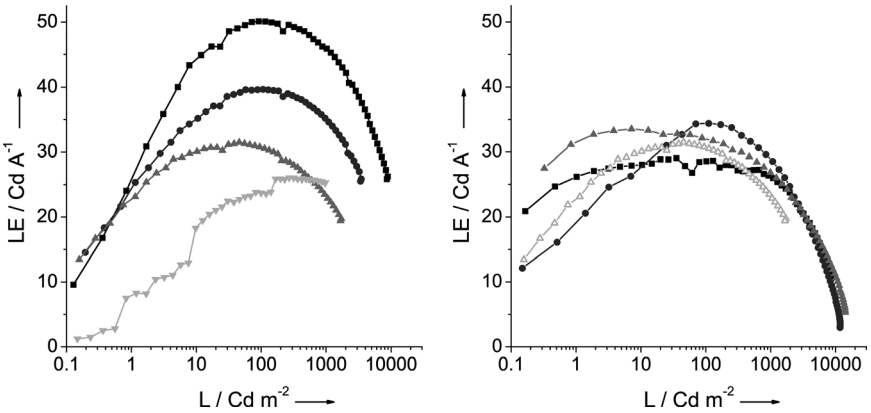

Figure 3. OLED Performance: Luminous efficiency (LE) as a function of luminance (L). Left: Devices P0–P3 consisting of PEDOT:PSS (35 nm)//X-TAPC (20 nm)//EML (80 nm)//CsF (2 nm)//Al (100 nm). The EML consisted of non-cross-linked X-IrG1 (squares: P1), X-IrG2 (circles: P2), X-IrG3 (up triangles: P3), *fac*-[Ir(mppy)$_3$] (down triangles: P0) as emitter in PVK/OXD-7 (5/67/28 wt%). Right: Devices S1 (closed, squares), S2 (closed, circles), and D (closed, up triangles); all devices contain cross-linked X-IrG3 as the emitter in the respective matrix (see Figure 2 for layer stack). For direct comparison, we have included the data for device P3 here as well (open, up triangles; same data is in Figure 3a).

our results show that the DEL concept works even in solution-processed devices.

The electroluminescence (EL) spectra (Figure S6) of the optimized devices show their maximum at 530 nm in all cases; slight differences occur in the intensity of the vibronic shoulder, leading to slight variations of the CIE color coordinates (Table S2). This is probably caused by different location, shape, and/or width of the emission zone (EMZ) inside the emitting layer.[14d,25] Note that the EL spectra were constant at all performance levels which indicates bipolar charge injection and transport into and through the EML independently of the drive voltage.

In conclusion, we report the synthesis and characterization of new cross-linkable green-emitting Ir^{III} complexes, which outperform solution-based polymeric PHOLEDs based on the commonly used reference compound *fac*-[Ir(mppy)$_3$] as a result of improved solubility and hole-transport properties. Luminous efficiencies of up to LE = 50 Cd A^{-1} and PE = 30 Lm W^{-1} (device P1, X-IrG1 in PVK/OXD-7) where achieved which is at least as efficient as devices fabricated by orthogonal solvent processing (53.8 Cd A^{-1} and 13.3 Lm W^{-1}),[11a] despite the fact that we did not use an additional ETL as was done in Ref.[11a]. Further, we introduced cross-linkable spirobifluorenes as host materials, which allowed the fabrication of the first solution-processed DEL–OLED, which reached a luminous efficiency of 33.5 Cd A^{-1} and a power efficacy of 30 Lm W^{-1}. This is more efficient than the reference device P3 and comparable to other green phosphorescent devices with solution-processed EML, although vacuum processed ETLs were used (30 Lm W^{-1}).[26]

Received: April 11, 2013
Revised: May 23, 2013
Published online: July 3, 2013

Keywords: cross-links · double-emission layers · iridium complexes · organic light-emitting diodes · solution processing

[1] a) L. Xiao, Z. Chen, B. Qu, J. Luo, S. Kong, Q. Gong, J. Kido, *Adv. Mater.* **2011**, *23*, 926 – 952; b) B. Geffroy, P. Le Roy, C. Prat, *Polym. Int.* **2006**, *55*, 572 – 582.

[2] a) M. A. Baldo, D. F. O'Brien, Y. You, A. Shoustikov, S. Sibley, M. E. Thompson, S. R. Forrest, *Nature* **1998**, *395*, 151 – 154; b) C. Cebrián, M. Mauro, D. Kourkoulos, P. Mercandelli, D. Hertel, K. Meerholz, C. A. Strassert, L. De Cola, *Adv. Mater.* **2013**, *25*, 437 – 442.

[3] M. A. Baldo, S. Lamansky, P. E. Burrows, M. E. Thompson, S. R. Forrest, *Appl. Phys. Lett.* **1999**, *75*, 4 – 6.

[4] C. Adachi, M. A. Baldo, M. E. Thompson, S. R. Forrest, *J. Appl. Phys.* **2001**, *90*, 5048 – 5051.

[5] H. Yersin, A. F. Rausch, R. Czerwieniec, T. Hofbeck, T. Fischer, *Coord. Chem. Rev.* **2011**, *255*, 2622 – 2652.

[6] T. Förster, *Ann. Phys.* **1948**, *437*, 55 – 75.

[7] D. L. Dexter, *J. Chem. Phys.* **1953**, *21*, 836 – 850.

[8] a) K. S. Yook, J. Y. Lee, *Adv. Mater.* **2012**, *24*, 3169 – 3190; b) Y. W. Park, J. H. Choi, T. H. Park, E. H. Song, H. Kim, H. J. Lee, S. J. Shin, B. K. Ju, W. J. Song, *Appl. Phys. Lett.* **2012**, *100*, 013312 ; c) S. L. Gong, X. He, Y. H. Chen, Z. Q. Jiang, C. Zhong, D. G. Ma, J. G. Qin, C. L. Yang, *J. Mater. Chem.* **2012**, *22*, 2894 – 2899; d) J. S. Chen, C. S. Shi, Q. Fu, F. C. Zhao, Y. Hu, Y. L. Feng, D. G. Ma, *J. Mater. Chem.* **2012**, *22*, 5164 – 5170; e) S. C. Lo, R. N. Bera, R. E. Harding, P. L. Burn, I. D. W. Samuel, *Adv. Funct. Mater.* **2008**, *18*, 3080 – 3090; f) J. W. Levell, S. Zhang, W. Y. Lai, S. C. Lo, P. L. Burn, I. D. W. Samuel, *Opt. Express* **2012**, *20*, A213 – A218.

[9] X. Zhou, D. S. Qin, M. Pfeiffer, J. Blochwitz-Nimoth, A. Werner, J. Drechsel, B. Maennig, K. Leo, M. Bold, P. Erk, H. Hartmann, *Appl. Phys. Lett.* **2002**, *81*, 4070 – 4072.

[10] C. M. Zhong, C. H. Duan, F. Huang, H. B. Wu, Y. Cao, *Chem. Mater.* **2011**, *23*, 326 – 340.

[11] a) T. Earmme, S. A. Jenekhe, *J. Mater. Chem.* **2012**, *22*, 4660 – 4668; b) X. Gong, S. Wang, D. Moses, G. C. Bazan, A. J. Heeger, *Adv. Mater.* **2005**, *17*, 2053 – 2058.

[12] a) B. W. Ma, B. J. Kim, D. A. Poulsen, S. J. Pastine, J. M. J. Frechet, *Adv. Funct. Mater.* **2009**, *19*, 1024 – 1031; b) N. Aizawa, Y. J. Pu, H. Sasabe, J. Kido, *Org. Electron.* **2013**, *14*, 1614 – 1620.

[13] a) C. D. Muller, K. Meerholz, O. Nuyken, *Organic Light-Emitting Devices*, *Vol. 1* (Ed.: U. S. K. Müllen), Wiley-VCH, Weinheim, **2005**, pp. 293 – 318; b) C. A. Zuniga, J. Abdallah, W. Haske, Y. Zhang, I. Coropceanu, S. Barlow, B. Kippelen, S. R. Marder, *Adv. Mater.* **2013**, *25*, 1739 – 1744.

[14] a) M. S. Bayerl, T. Braig, O. Nuyken, D. C. Muller, M. Gross, K. Meerholz, *Macromol. Rapid Commun.* **1999**, *20*, 224 – 228; b) C. D. Müller, T. Braig, H. G. Nothofer, M. Arnoldi, M. Gross, U. Scherf, O. Nuyken, K. Meerholz, *ChemPhysChem* **2000**, *1*, 207 – 211; c) P. Zacharias, M. C. Gather, M. Rojahn, O. Nuyken, K. Meerholz, *Angew. Chem.* **2007**, *119*, 4467 – 4471; *Angew. Chem. Int. Ed.* **2007**, *46*, 4388 – 4392; d) G. Liaptsis, K. Meerholz, *Adv. Funct. Mater.* **2013**, *23*, 359 – 365; e) J. Schelter, G. F. Mielke, A. Kohnen, J. Wies, S. Kober, O. Nuyken, K. Meerholz, *Macromol. Rapid Commun.* **2010**, *31*, 1560 – 1567; f) C. D. Müller, A. Falcou, N. Reckefuss, M. Rojahn, V. Wiederhirn, P. Rudati, H. Frohne, O. Nuyken, H. Becker, K. Meerholz, *Nature* **2003**, *421*, 829 – 833; g) M. C. Gather, A. Kohnen, A. Falcou, H. Becker, K. Meerholz, *Adv. Funct. Mater.* **2007**, *17*, 191 – 200.

[15] a) A. Nakamura, T. Tada, M. Mizukami, S. Yagyu, *Appl. Phys. Lett.* **2004**, *84*, 130 – 132; b) X. H. Yang, D. Neher, D. Hertel, T. K. Daubler, *Adv. Mater.* **2004**, *16*, 161 – 166; c) M. K. Mathai, V. E. Choong, S. A. Choulis, B. Krummacher, F. So, *Appl. Phys. Lett.* **2006**, *88*, 243512; d) X. H. Yang, D. C. Muller, D. Neher, K. Meerholz, *Adv. Mater.* **2006**, *18*, 948 – 954.

[16] W. G. Zhu, Y. Q. Mo, M. Yuan, W. Yang, Y. Cao, *Appl. Phys. Lett.* **2002**, *80*, 2045 – 2047.

[17] H. Yersin, *Top. Curr. Chem.* **2004**, *241*, 1 – 26.

[18] a) F. Laquai, D. Hertel, *Appl. Phys. Lett.* **2007**, *90*, 142109; b) H. A. Al Attar, A. P. Monkman, *Adv. Funct. Mater.* **2006**, *16*, 2231 – 2242.

[19] a) T. Tsuzuki, S. Tokito, *Appl. Phys. Lett.* **2009**, *94*, 033302; b) S. O. Jeon, K. S. Yook, C. W. Joo, J. Y. Lee, *Org. Electron.* **2010**, *11*, 881 – 886; c) J. Zhao, G. H. Xie, C. R. Yin, L. H. Xie, C. M. Han, R. F. Chen, H. Xu, M. D. Yi, Z. P. Deng, S. F. Chen, Y. Zhao, S. Y. Liu, W. Huang, *Chem. Mater.* **2011**, *23*, 5331 – 5339.

[20] Y. L. Liao, C. Y. Lin, Y. H. Liu, K. T. Wong, W. Y. Hung, W. J. Chen, *Chem. Commun.* **2007**, 1831 – 1833.

[21] a) N. J. Turro, *Modern Molecular Photochemistry*, University Science Books, Sausalito, **1991**; b) B. Milián-Medina, J. Gierschner, *Org. Electron.* **2012**, *13*, 985 – 991.

[22] a) R. Pudzich, T. Fuhrmann-Lieker, J. Salbeck, *Adv. Polym. Sci.* **2006**, *199*, 83 – 142; b) T. P. Saragi, T. Spehr, A. Siebert, T. Fuhrmann-Lieker, J. Salbeck, *Chem. Rev.* **2007**, *107*, 1011 – 1065.

[23] M. A. Baldo, C. Adachi, S. R. Forrest, *Phys. Rev. B* **2000**, *62*, 10967 – 10977.

[24] D. Hertel, K. Meerholz, *J. Phys. Chem. B* **2007**, *111*, 12075 – 12080.

[25] S. Reineke, K. Walzer, K. Leo, *Phys. Rev. B* **2007**, *75*, 125328.

[26] N. Aizawa, Y. J. Pu, H. Sasabe, J. Kido, *Org. Electron.* **2012**, *13*, 2235 – 2242.
[27] J. Lee, N. Chopra, S. H. Eom, Y. Zheng, J. G. Xue, F. So, J. M. Shi, *Appl. Phys. Lett.* **2008**, *93*, 123306.
[28] J. Pina, J. S. de Melo, H. D. Burrows, A. P. Monkman, S. Navaratnam, *Chem. Phys. Lett.* **2004**, *400*, 441 – 445.
[29] K. T. Wong, S. Y. Ku, Y. M. Cheng, X. Y. Lin, Y. Y. Hung, S. C. Pu, P. T. Chou, G. H. Lee, S. M. Peng, *J. Org. Chem.* **2006**, *71*, 456 – 465.

